Model Predictive Control of 5L-ANPC Inverter Fed Coreless AFPM Motor with Mitigated CMV in Electric Aircraft Propulsion

Farzad Y. Notash, Matin Vatani, JiangBiao He, and Dan M. Ionel
Department of Electrical and Computer Engineering
University of Kentucky
Lexington, KY, USA
Emails: farzad.y.notash@uky.edu, matin.vatani@uky.edu, jiangbiao@ieee.org, and dan.ionel@ieee.org

***Abstract*—This paper proposes a fast model predictive control (FMPC) method without weighting factors and mitigated common-mode voltage (CMV) for a five-level active neutral point clamped (5L-ANPC) inverter-fed electric aircraft propulsion system with a coreless axial flux permanent magnet (CAFPM) motor. This motor is specifically designed for electric aircraft propulsion through a combined electromagnetic and thermal evaluation, benefiting from a high specific power density, efficiency, and integrated thermal management system. The proposed method utilizes the deadbeat approach to calculate the reference voltage vector and compensate for the one-time interval delay between the predicted and applied switching commands. The angle and amplitude of the reference voltage vector in the inverter's space vector diagram are utilized to find the optimum voltage vector from a series of candidate voltage vectors with mitigated CMV values to one-sixth of the DC-link voltage. Moreover, hierarchical cost functions without weighting factors are adopted to achieve multi-objective optimizations and predict the optimum switching state. Compared to the conventional MPC method, the proposed method requires significantly shorter calculation time, leading to utilizing high sampling frequencies and improving the steady-state and dynamic performance of the motor-drive system. The performance of the proposed method is investigated in the takeoff and cruise modes of an electric aircraft's mission profile.**

***Index Terms*—Model predictive control, 5L-ANPC inverter, coreless axial flux permanent magnet motor, common-mode voltage, electric aircraft propulsion.**

I. Introduction

Over the past decade, the aviation industry has made remarkable progress in developing hybrid/electric aircraft, owing to their desirable benefits, including near-zero emissions, reduced operational costs, lower noise pollution, and enhanced efficiency [1], [2]. Concurrently, distributed electric propulsion (DEP) systems are being explored to maximize these advantages. DEP systems comprise multiple small electric propulsion units positioned along the aircraft's wings to help increase the energy efficiency and enhance aerodynamics [3].

Hybrid/electric aircraft require electric motors with high efficiency and torque density. Recently, axial flux permanent magnet (AFPM) motors have attracted attention in such applications. AFPM motors can provide high specific power density and a compact design compared to their radial flux motor counterparts [4], [5]. The axial flux configuration allows multiple units to be integrated on a single shaft, resulting in greater compactness, since radial flux designs have volumetric overhead from the two sets of the end windings in the central area [6].

Among the various AFPM motor topologies, coreless AFPM (CAFPM) motors offer additional benefits, including potentially higher power density, reduced vibration, and increased efficiency [7]. Unlike the conventional cored motors, where the windings are located within stator slots, CAFPM machines have better access to the windings, enabling more convenient cooling.

The five-level active neutral point clamped (5L-ANPC) power converter has been widely used in high-power medium-voltage motor drives. Its topology allows higher voltages than the voltage ratings of its semiconductor devices can withstand. Also, 5L-ANPC inverter exhibits lower $\frac{dv}{dt}$, reduced semiconductor losses, and increased power quality [8].

Conventional 5L-ANPC inverter-fed motor-drive systems have a hierarchical control strategy, where the first layer includes a motor control algorithm like field-oriented control (FOC) or direct torque control (DTC), and the second layer involves a modulation technique such as carrier-based pulse-width modulation (PWM) or space vector modulation (SVM). In the case of the 5L-ANPC inverters, the former has inherently limited utilization of the DC-link voltage and complex calculations for the necessary zero-sequence voltage. On the other hand, the latter technique is more intricate and demands more intensive computation [9]. Furthermore, the adopted modulation technique should provide a balanced voltage over the DC-link and flying capacitors of the inverter.

In addition to ensuring precise speed/torque control and balancing the DC-link and flying capacitor voltages in 5L-ANPC-fed high-power motor-drive systems, addressing the issue of common-mode voltage (CMV) is crucial. CMV can cause high motor bearing voltage and currents, leading to degraded motor bearing insulation [10]. Mitigating CMV also helps reduce the motor-drive system's electromagnetic interference (EMI), which is especially more challenging for inverters consisting

This research is funded by the NASA University Leadership Initiative (ULI) program #80NSSC22M0068.

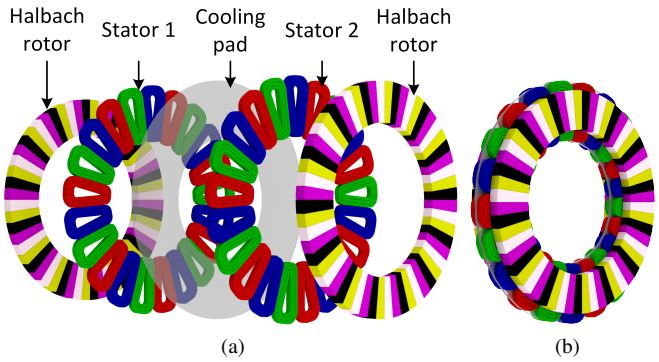

Fig. 1. Coreless AFPM machine with a double-sided Halbach PM array rotor and an axial feature of direct cooling between stators for electric aircraft propulsion, showing (a) an exploded view and (b) a compact view.

of fast-switching Silicon Carbide (SiC) and Gallium Nitride (GaN) transistors.

The model predictive control (MPC) method is a promising control method for motor-drive systems and has been extensively studied over the past two decades. It simplifies the control process by directly providing gate signals to the semiconductor switches of the inverter. The MPC method is intuitively straightforward and excels over the FOC and DTC methods due to its ability to handle multi-objective optimization problems and system nonlinearities. The finite control set - MPC (FCS-MPC) method is the most popular among the various MPC methods. It involves an iterative search to predict the future behaviors of selected state variables for all possible switching states of the inverter. The optimal switching state is then chosen by minimizing a non-zero cost function and applied to the inverter [11].

Implementing the conventional MPC method for motor-drive systems with 5L-ANPC inverters imposes a high computational burden due to the iterative search among 512 switching states. Additionally, balancing the voltages across the DC-link and flying capacitors while maintaining desirable control performance is also difficult due to the trade-off involved in tuning the weighting factors in the cost function [12].

This paper proposes a method that addresses the challenges of using the MPC method in CAFPM motor-drive systems with 5L-ANPC inverters. The contributions of this paper are as follows: (1) Instead of using 512 switching states in the iterative search algorithm, only 61 voltage vectors with mitigated CMV values are used. (2) The computational burden originating from a large number of switching states is dramatically reduced by choosing 10 or 9 candidate voltage vectors through a deadbeat approach. (3) By hierarchical cost functions without weighting factors, firstly, the optimum voltage vector is selected, and secondly, its switching states are evaluated to balance the DC-link and flying capacitor voltages.

II. Coreless AFPM Motor

A. Topology and Characteristics

A CAFPM motor with the potential for high specific power was proposed and designed for electric aircraft propulsion, as outlined in [13]. The motor delivers a rated power of 1.5 MW at 3000 rpm, within a 500 mm outer diameter imposed by the aircraft body design. The topology of the proposed CAFPM motor, including the electromagnetic components and the integrated direct cooling structure, is illustrated in Fig. 1.

The proposed CAFPM motor utilizes a double-sided Halbach permanent magnet (PM) array rotor, which offers enhanced specific power capability compared to the conventional surface-mounted variant. The Halbach rotor features four PMs for every 360 electrical degree, arranged in a 90-degree configuration. This arrangement eliminates the need for a rotor back iron for flux path return.

The Halbach PM array rotor generates over 30% more torque compared to a surface-mounted rotor of identical size and mass. However, this increased performance comes with a significantly higher cost due to the additional PM material and the more complex mechanical structure. For electric aircraft propulsion, where specific power capability is prioritized over cost, the Halbach PM array rotor is a more suitable choice.

The stator features two sets of three-phase windings, each connected to a separate inverter to improve fault tolerance. These windings are arranged in a concentrated pattern with a coil pitch of 240 electrical degrees. The direct exposure of the windings to magnetic field harmonics from the rotor induces eddy currents in the conductors. In order to mitigate these eddy current losses, rectangular Litz wire with very thin conductors and fine transposition is used.

Eliminating the stator core can potentially enhance the specific power and efficiency of motors. This leads to a motor with lower phase inductance than conventional cored motors and with equal direct and quadrature inductance. Due to the low phase inductance, both current and torque ripple may increase, which can be mitigated by using a high switching frequency. Additionally, the large moment of inertia imposed by the propeller in electric aircraft can naturally reduce torque ripple to a significant extent.

An axial direct cooling feature, a cooling pad, is incorporated between the two stators to support higher current density values. The cooling pad material is non-ferromagnetic to avoid affecting the magnetic flux path and non-conductive to prevent eddy current losses. A cryogenic coolant will circulate within the cooling pad to dissipate heat loss from the stator windings.

B. Dynamic Model of Coreless AFPM Motor

In order to implement the FCS-MPC method, the dynamic model of the motor-drive system is required. By ignoring the hysteresis eddy currents and magnetic circuit saturation, the dq stator voltage equations of a CAFPM motor are [4]:

$$\begin{aligned} u_d &= R_s i_d + L_d \frac{di_d}{dt} - \omega_e L_q i_q \\ u_q &= R_s i_q + L_q \frac{di_q}{dt} + \omega_e L_d i_d + \omega_e \psi_f \end{aligned} \tag{1}$$

where i_{dq} is the dq stator current vector, R_s is the stator resistance, L_d and L_q are the dq stator inductances, ω_e is the electrical angular speed, and ψ_f is the flux linkage.

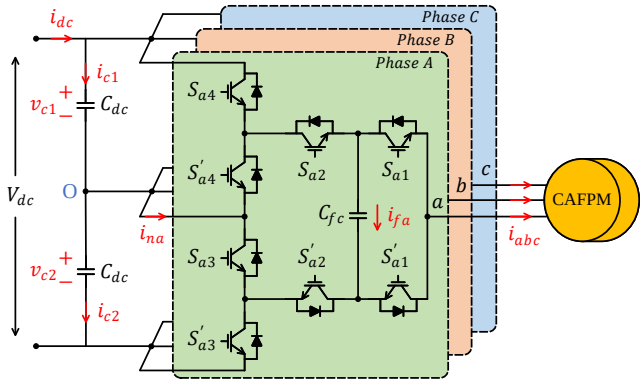

Fig. 2. The 5L-ANPC inverter-fed CAFPM motor-drive system [12].

TABLE I
SWITCHING STATES OF THE 5L-ANPC INVERTER

Switching States	S_{x1}	S_{x3}	S_{x4}	i_{nx}	i_{fx}	u_{xo}
V_0	0	0	0	0	0	$\frac{-V_{dc}}{2}$
V_1	0	0	1	0	$-i_x$	$\frac{-V_{dc}}{4}$
V_2	0	1	0	i_x	i_x	$\frac{-V_{dc}}{4}$
V_3	0	1	1	i_x	0	0
V_4	1	0	0	i_x	0	0
V_5	1	0	1	i_x	$-i_x$	$\frac{V_{dc}}{4}$
V_6	1	1	0	0	i_x	$\frac{V_{dc}}{4}$
V_7	1	1	1	0	0	$\frac{V_{dc}}{2}$

III. 5L-ANPC Inverter

Fig. 2 depicts the circuit topology of a 5L-ANPC inverter-fed CAFPM motor-drive system. This inverter has two DC-link capacitors, and each phase of the inverter has eight switches and one flying capacitor. The DC-link and flying capacitor voltages are balanced at $\frac{V_{dc}}{2}$ and $\frac{V_{dc}}{4}$, respectively. Switches (S_1, $S_1^{'}$), (S_2, $S_2^{'}$), (S_3, $S_3^{'}$), and (S_4, $S_4^{'}$) are complementary. Table I summarizes the switching states of the 5L-ANPC inverter. Switches S_1 and S_2 are switched ON and OFF simultaneously. Based on its various ON and OFF switching combinations, each phase of this inverter produces 8 switching states and 5 voltage vectors u_{xo} with 5 distinct voltage levels, where $x \in \{a, b, c\}$. Therefore, $8^3 = 512$ switching states and $5^3 = 125$ voltage vectors are generated in total. In addition, the neutral point currents i_{nx} and flying capacitor currents i_{fx} are presented for various switching states. Based on Table I, the five generated per-phase voltage levels of this inverter are $\frac{-V_{dc}}{2}$, $\frac{-V_{dc}}{4}$, 0, $\frac{V_{dc}}{4}$, and $\frac{V_{dc}}{2}$, which are denoted as "0", "1", "2", "3", and "4", respectively [12].

IV. Conventional Model Predictive Control (CMPC) Method

In the MPC method based motor-drive systems, the dq stator current vector is usually selected as the state variable to control the motor's rotational speed and electromagnetic torque. By applying the Forward Euler approximation method on (1), the discrete-time mathematical model of the CAFPM motor is obtained to predict the dq stator current vector [14].

$$\begin{aligned} i_d^{k+1} &= \left(1 - \frac{R_s T_s}{L_d}\right) i_d^k + \frac{T_s}{L_d} u_d^k + \frac{T_s \omega_e^k L_q}{L_d} i_q^k \\ i_q^{k+1} &= \left(1 - \frac{R_s T_s}{L_q}\right) i_q^k + \frac{T_s}{L_q} u_q^k - \frac{T_s \omega_e^k L_d}{L_q} i_d^k - \frac{T_s \omega_e^k \psi_f}{L_q} \end{aligned} \tag{2}$$

where T_s is the sampling time, k is the sampling interval, i_{dq}^{k+1} is the predicted dq stator current vector, i_{dq}^k is the measured dq stator current vector, u_{dq}^k is the applied dq stator voltage vector, and ω_e^k is the measured electrical angular speed. In other words, the dq stator current vector is predicted for all generated dq stator voltage vectors of the inverter in the conventional MPC (CMPC) method. Meanwhile, the DC-link and flying capacitor voltages should be balanced. The redundant switching states of the inverter have different charging/discharging effects on the voltage values of the DC-link and flying capacitors. Hence, their voltage values should be predicted for all possible u_{dq}^k of the inverter. Firstly, their predicted current values should be calculated at instance $k+1$.

$$\begin{aligned} i_{c1}^{k+1} &= i_{dc} - S_{a4}S_{a2}i_a - S_{b4}S_{b2}i_b - S_{c4}S_{c2}i_c \\ i_{c2}^{k+1} &= i_{dc} + S_{a3}^{'}S_{a2}^{'}i_a + S_{b3}^{'}S_{b2}^{'}i_b + S_{c3}^{'}S_{c2}^{'}i_c \end{aligned} \tag{3}$$

$$\begin{aligned} i_{fa}^{k+1} &= (S_{a2} - S_{a1})i_a \\ i_{fb}^{k+1} &= (S_{b2} - S_{b1})i_b \\ i_{fc}^{k+1} &= (S_{c2} - S_{c1})i_c \end{aligned} \tag{4}$$

where i_a, i_b, and i_c are the measured stator phase currents, and i_{dc} is the measured DC-bus current. Then, their predicted voltage values at instance $k+1$ can be calculated:

$$v_{cn}^{k+1} = v_{cn}^k + \frac{T_s}{C_{dc}} i_{cn}^{k+1} \tag{5}$$

$$v_{fx}^{k+1} = v_{fx}^k + \frac{T_s}{C_{fc}} i_{fx}^{k+1} \tag{6}$$

where $n \in \{1, 2\}$ and $x \in \{a, b, c\}$, and C_{dc} and C_{fc} are the DC-link capacitance and flying capacitance, respectively. Finally, the multi-objective cost function C of the CMPC method is formulated using (2), (5), and (6) [12].

$$\begin{aligned} C = &\left(i_d^* - i_d^{k+1}\right)^2 + \left(i_q^* - i_q^{k+1}\right)^2 \\ &+ \lambda_{dc}\left(\frac{Vdc}{2} - v_{cn}^{k+1}\right)^2 + \lambda_{fc}\left(\frac{Vdc}{4} - v_{fx}^{k+1}\right)^2 \end{aligned} \tag{7}$$

where i_{dq}^* is the reference dq stator current vector, and λ_{dc} and λ_{fc} are, respectively, the weighting factors of the terms responsible for balancing the voltage of the DC-link and flying capacitors. In the CMPC method, all 512 switching states of the 5L-ANPC inverter are utilized in an exhaustive approach to calculate (7). The switching state that minimizes (7) is selected and directly applied to the switches. The control diagram of the CMPC method with delay compensation is illustrated in Fig. 3. The measured phase currents are transformed into the dq reference frame. The stator current vector i_{dq}, DC-link

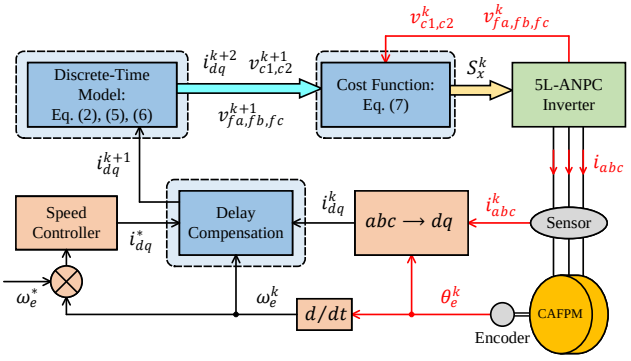

Fig. 3. Control diagram of the conventional MPC (CMPC) [12].

capacitor voltages, and flying capacitor voltages are predicted for all 512 switching states. Finally, the multi-objective cost function C is evaluated, and the optimum switching state is applied to the inverter.

V. Proposed Fast MPC (FMPC) Method with Mitigated Common-Mode Voltage (CMV)

The CMPC-based motor-drive systems perform an exhaustive search algorithm across all possible switching states of the inverter to find the optimum one. With 512 switching state combinations of the 5L-ANPC inverter, the CMPC method becomes computationally burdensome. As a result, large values of T_s are necessary to cover the required computational time for such burdensome calculations. Using large values of T_s results in various challenges. Firstly, it leads to lower switching frequencies. Secondly, the steady-state and dynamic performance of the motor-drive system may become undesirable due to induced high rotational speed and electromagnetic torque ripples. Additionally, dealing with multiple weighting factors in the multi-objective cost function of the CMPC method often results in a trade-off among various control objectives. Furthermore, to address the CMV mitigation, adding another term to (7) leads to further challenges in the trade-off mentioned above. The proposed Fast MPC (FMPC) effectively addresses these challenges through three main steps detailed as follows.

A. Step One: Deadbeat Approach

The first step of the proposed FMPC reduces the computational burden of the iterative search algorithm by reducing its number of calculations. Thus, the discrete-time dq stator voltage vector of the CAFPM motor is obtained [14], [15].

$$u_d^{k+1} = \frac{L_d}{T_s}\left(i_d^* + \left(\frac{T_s R_s}{L_d}\right) i_d^{k+1}\right) - \omega_e^k L_q i_q^{k+1}$$
$$u_q^{k+1} = \frac{L_q}{T_s}\left(i_q^* + \left(\frac{T_s R_s}{L_q}\right) i_q^{k+1}\right) - \omega_e^k L_d i_d^{k+1} + \omega_e^k \psi_f \tag{8}$$

where i_{dq}^* is the reference dq stator current vector and ω_e^k is assumed to be constant during the intervals ($\omega_e^{k+1} \simeq \omega_e^k$). Moreover, u_{dq}^{k+1} is the dq stator voltage vector by which the dq stator current vector at instance $k+1$ tracks its reference value at instance $k+2$. Hence, u_{dq}^{k+1} is considered as the reference dq voltage vector.

$$u_{dq}^* = u_{dq}^{k+1} \tag{9}$$

By doing so, one sampling delay caused by implementing the MPC method is compensated by estimating i_{dq}^{k+1} in (2) through adopting u_{dq}^k from instance $k-1$. Finally, the reference $\alpha\beta$ voltage vector $u_{\alpha\beta}^*$ is calculated using the Inverse-Park transformation:

$$\begin{bmatrix} u_\alpha^* \\ u_\beta^* \\ 0 \end{bmatrix} = \begin{bmatrix} \cos\theta_e & -\sin\theta_e & 0 \\ \sin\theta_e & \cos\theta_e & 0 \\ 0 & 0 & 1 \end{bmatrix} \begin{bmatrix} u_d^* \\ u_q^* \\ 0 \end{bmatrix} \tag{10}$$

where θ_e is the electrical rotational angle. The angle of $u_{\alpha\beta}^*$ is used in the second and third steps of the proposed FMPC to select the optimum voltage vector.

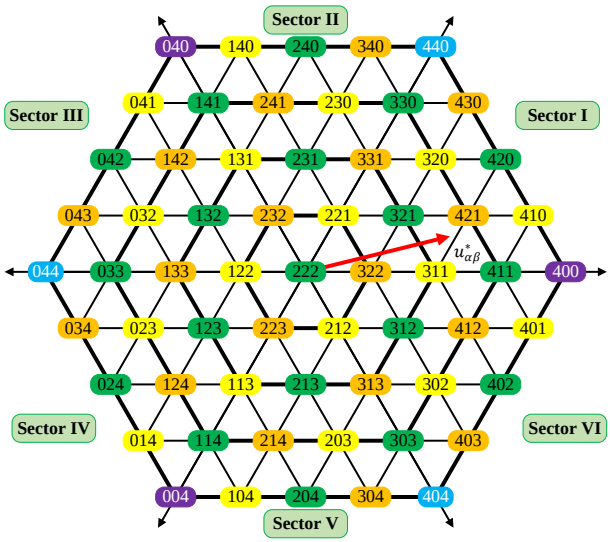

Fig. 4. Space vector of the 5L-ANPC inverter with 61 candidate voltage vectors of the proposed FMPC.

B. Step Two: CMV Mitigation

The second step of the proposed FMPC aims to reduce the computational burden and mitigate the CMV. For the wye connection of the three-phase stator windings of the motor, the CMV value is formulated as [10]:

$$CMV = \frac{u_{ao} + u_{bo} + u_{co}}{3} \tag{11}$$

The 5L-ANPC inverter generates 125 voltage vectors with 13 distinct values of CMV, which are "$\frac{-V_{dc}}{2}$", "$\frac{-5V_{dc}}{12}$", "$\frac{-V_{dc}}{3}$", "$\frac{-V_{dc}}{4}$", "$\frac{-V_{dc}}{6}$", "$\frac{-V_{dc}}{12}$", 0, "$\frac{V_{dc}}{12}$","$\frac{V_{dc}}{6}$", "$\frac{V_{dc}}{4}$", "$\frac{V_{dc}}{3}$", "$\frac{2V_{dc}}{12}$", and "$\frac{V_{dc}}{2}$". Inspired by [16], the proposed FMPC utilizes only 61 voltage vectors with mitigated values of CMV, i.e., the voltage vectors with CMV values of "$\frac{-V_{dc}}{2}$", "$\frac{-5V_{dc}}{12}$", "$\frac{-V_{dc}}{3}$", "$\frac{-V_{dc}}{4}$", "$\frac{V_{dc}}{4}$", "$\frac{V_{dc}}{3}$" "$\frac{5V_{dc}}{12}$", and "$\frac{V_{dc}}{2}$" are eliminated in the iterative search algorithm. The space vector of the 5L-ANPC inverter with the remaining 61 voltage vectors is shown in Fig. 4 in the $\alpha\beta$ reference frame. The 'purple'

TABLE II
CMV VALUES OF THE 61 VOLTAGE VECTORS IN THE PROPOSED FMPC

CMV Values	Candidate Voltage Vectors
$\frac{-V_{dc}}{6}$	(040), (400), (004)
$\frac{-V_{dc}}{12}$	(140), (041), (230), (131), (320), (032), (221), (410), (122), (311), (023), (212), (401), (113), (302), (014), (203), (104)
0	(240), (141), (330), (042), (231), (420), (132), (321), (033), (222), (411), (123), (312), (024), (213), (402), (114), (303), (204)
$\frac{V_{dc}}{12}$	(340), (241), (430), (142), (331), (043), (232), (421), (133), (322), (034), (223), (412), (124), (313), (214), (403), (304)
$\frac{V_{dc}}{6}$	(440), (044), (404)

TABLE III
RELATIONSHIP BETWEEN THE ANGLE OF $u^*_{\alpha\beta}$ AND SECTORS IN THE SPACE VECTOR DIAGRAM OF THE 5L-ANPC INVERTER

The Angle of $u^*_{\alpha\beta}$	Optimum Sector
$0 \leq \theta^*_{\alpha\beta} < 60$	I
$60 \leq \theta^*_{\alpha\beta} < 120$	II
$120 \leq \theta^*_{\alpha\beta} < 180$	III
$180 \leq \theta^*_{\alpha\beta} < 240$	IV
$240 \leq \theta^*_{\alpha\beta} < 300$	V
$300 \leq \theta^*_{\alpha\beta} < 360$	VI

and 'blue' voltage vectors have the CMV values of "$\frac{-V_{dc}}{6}$" and "$\frac{V_{dc}}{6}$", respectively. The CMV values for the 'yellow' and 'orange' voltage vectors are, respectively, "$\frac{-V_{dc}}{12}$" and "$\frac{V_{dc}}{12}$". The 'green' voltage vectors have the CMV value of 0. Table II categorizes the adopted 61 candidate voltage vectors in the proposed FMPC according to their CMV values.

In order to further reduce the computational burden, the space vector of the 5L-ANPC inverter in Fig. 4 is divided into 6 sectors. According to Table III, the angle of $u^*_{\alpha\beta}$, namely $\theta^*_{\alpha\beta}$, from the first step is used to determine the optimum sector. Afterwards, each sector is divided into two sub-sectors. For instance, the two sub-sectors for Sector I are depicted in Fig. 5. If the magnitude of $u^*_{\alpha\beta}$, satisfies the conditions in (12), the 'Gray' sub-sector is selected. Otherwise, the 'white' sub-sector is taken.

$$|u^*_\alpha| \leq \frac{V_{dc}}{4} \qquad |u^*_\beta| \leq \frac{V_{dc}}{4} \qquad \frac{V_{dc}}{4} - |u^*_\beta| \geq \frac{|u^*_\alpha|}{\sqrt{3}} \tag{12}$$

C. Step Three: Hierarchical Cost Function

When the optimum sub-sector is determined in the second step, only its associated voltage vectors are utilized in the search algorithm of the proposed FMPC. For example, the associated voltage vectors of the two sub-sectors in Fig. 5 are presented in Table IV. By doing so, only 10 and 9 candidate voltage vectors are, respectively, adopted for the 'gray' and 'white' sub-sectors, resulting in a further reduction of the calculation time. In the third step, a hierarchical cost function is utilized for eliminating the weighting factors of (7).

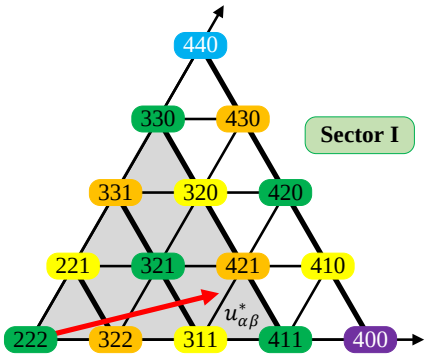

Fig. 5. Space vector of the 5L-ANPC inverter with 61 candidate voltage vectors of the proposed FMPC.

TABLE IV
CANDIDATE VOLTAGE VECTORS ASSOCIATED WITH THE TWO SUB-SECTORS OF SECTOR I

Sub-Sectors of Sector I	Candidate Voltage Vectors
The 'Gray' Sub-Sector	(222), (322), (311), (411), (221), (321), (421), (331), (320), (330)
The 'White' Sub-Sector	(411), (400), (421), (410), (320), (420), (330), (430), (440)

$$C_1 = (u^*_d - u^k_d)^2 + (u^*_q - u^k_q)^2 \tag{13}$$

$$C_2 = \left(\frac{Vdc}{2} - v^{k+1}_{cn}\right)^2 + \left(\frac{Vdc}{4} - v^{k+1}_{fx}\right)^2 \tag{14}$$

Firstly, the optimum voltage vector is selected using (13) by performing an iterative search among the associated candidate voltage vectors of the optimum sub-sector from Table IV. The candidate voltage vector leading to the least value of (13) is selected as the optimum one. By applying the determined optimum voltage vector, i_{dq} will follow its reference value. Therefore, various possible switching states of the optimum voltage vector yield the same dynamic performance. However, the optimum switching state is selected using (14), which provides a balanced voltage over the DC-link and flying capacitors. Such an approach of the proposed FMPC eliminates the weighting factors and reduces the number of calculations from 512 to at most 18. Fig. 6 illustrates the control diagram of the proposed FMPC with its described three major steps.

VI. SIMULATION ANALYSIS

An electric aircraft propulsion system with the CAFPM motor introduced in Section II-A is adopted for the simulation studies. The rated parameters of this motor are presented in Table V with an inverter dc-bus voltage of $V_{dc} = 800V$. Any aircraft flight mission profile consists of various modes such as acceleration, takeoff, cruise, landing, etc. However, the most

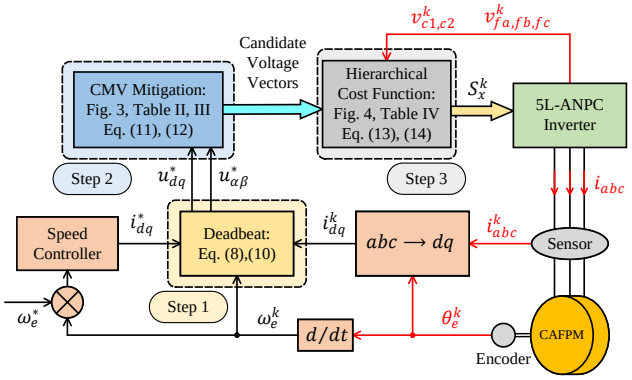

Fig. 6. Control diagram of the proposed fast MPC (FMPC).

TABLE V
PARAMETERS OF THE CAFPM MOTOR

Parameter	Value
Rated Power $[MW]$	1.5
Rated Speed $[rpm]$	3000
Fundamental Frequency $[Hz]$	800
Phase Resistance [p.u.]	0.04
Self Inductance [p.u.]	0.35

prominent modes are the takeoff and cruise modes, which are taken in this study. Additionally, since the introduced CAFPM motor has a low per-unit inductance, it may have a high phase current and electromagnetic torque ripples. This issue is primarily induced by the motor-drive system and can be addressed by either operating at relatively high switching frequencies or incorporating line filter inductance L_f. Since the proposed FMPC method has a significantly lower computational burden than the CMPC method, it can take very low sampling time to enhance the steady-state performance. Furthermore, an $L_f = 0.3$ p.u. is used, and its associated results are compared with those obtained without L_f.

A. Case 1: Takeoff Mode

The assumed reference speed and torque values are 1 per unit in the takeoff mode. A comparative study of the proposed FMPC method with and without L_f is presented in the takeoff mode. Fig. 7 shows that the speed ripple with the proposed method is desirably low and remains almost the same regardless of L_f. According to Fig. 8, the torque ripple is almost 16% with L_f. The steady-state 3-phase stator currents are illustrated in Fig. 9, showing that the current total harmonic distortion (THD) with line filter inductance is 3%. Similarly, according to Fig. 10 and Fig. 11, the i_q and i_d ripples are lower in case of adding L_f. Meanwhile, Fig. 12 and Fig. 13 verify that the voltages of the DC-link and flying capacitors are, respectively, balanced at $\frac{V_{dc}}{2}$ and $\frac{V_{dc}}{4}$ with the proposed method. However, adding the line filter inductance does not affect their ripples.

B. Case 2: Cruise Mode

The performance of the proposed FMPC method with and without L_f is investigated in cruise mode, where the reference speed and torque values are 0.95 and 0.51 p.u., respectively. The same studies as section VI-A are conducted. Based on Fig. 14, the proposed method's reference speed tracking performance is desirably low. Fig. 15 shows that

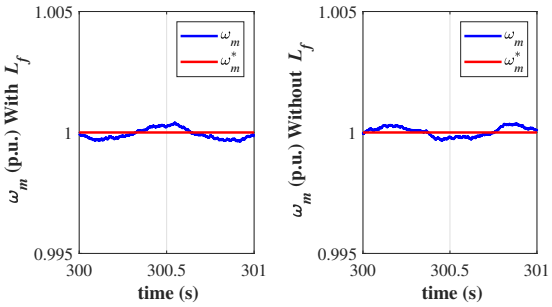

Fig. 7. Case 1: Steady-state speed ripple of the FMPC with/without L_f.

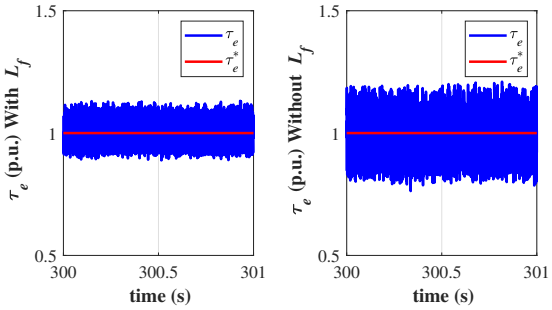

Fig. 8. Case 1: Steady-state torque ripple of the FMPC with/without L_f.

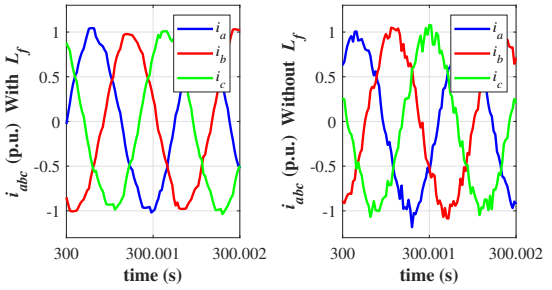

Fig. 9. Case 1: Three-phase current ripple of the FMPC with/without L_f.

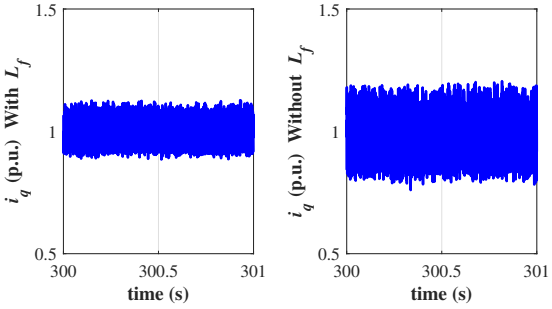

Fig. 10. Case 1: i_q ripple of the FMPC with/without L_f.

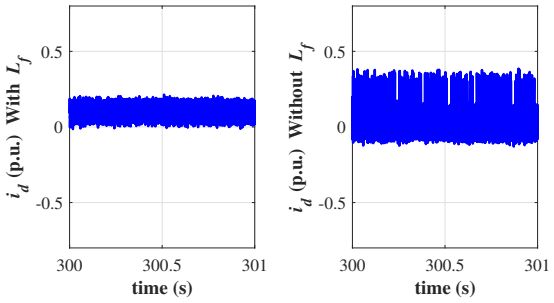

Fig. 11. Case 1: i_d ripple of the FMPC with/without L_f.

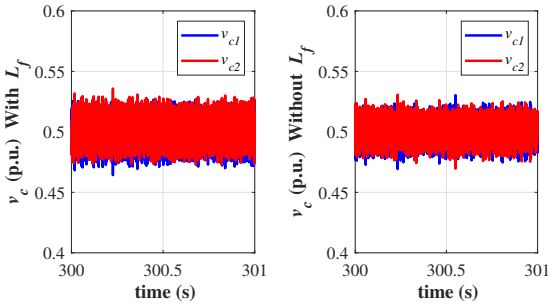

Fig. 12. Case 1: DC-link capacitor ripple of the FMPC with/without L_f.

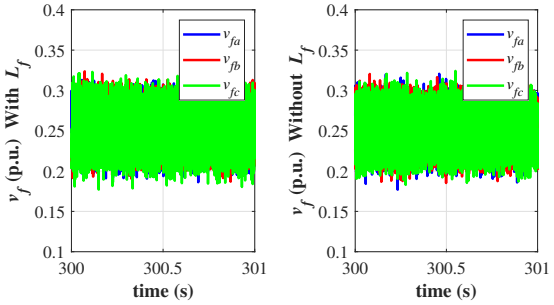

Fig. 13. Case 1: Flying capacitor ripple of the FMPC with/without L_f.

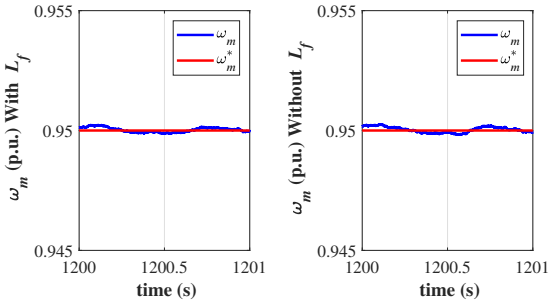

Fig. 14. Case 2: Steady-state speed ripple of the FMPC with/without L_f.

the reference torque tracking ripple is almost 19% with L_f. Like the previous case, Fig. 16 verifies that the phase current ripple is lower with line filter inductance. Fig. 10 and Fig. 11 respectively show that the i_q and i_d ripples are lower when L_f is added. Fig. 19 and Fig. 20 respectively verify that the voltages of the DC-link and flying capacitors in the proposed method are balanced at half and one-quarter of the DC-link voltage with relatively lower ripples compared to the Case 1.

C. CMV Mitigation

In this section, the CMV values of the CMPC and proposed FMPC methods are compared. According to Fig. 21, the CMV value with the proposed FMPC method is effectively limited to $\pm\frac{V_{dc}}{6}$. This is due to having a set of 61 voltage vectors with mitigated CMV values instead of the initial 125 ones in the proposed method. Furthermore, the CMV frequency is fixed to the sampling frequency of the proposed method.

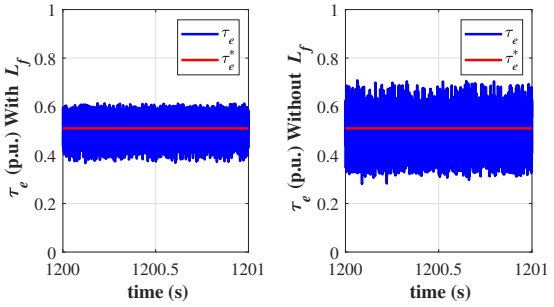

Fig. 15. Case 2: Steady-state torque ripple of the FMPC with/without L_f.

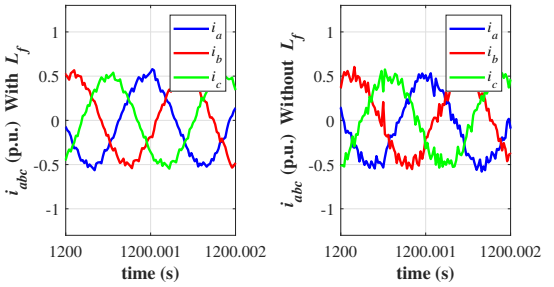

Fig. 16. Case 2: Three-phase current ripple of the FMPC with/without L_f.

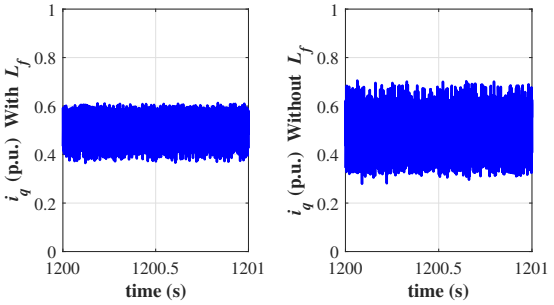

Fig. 17. Case 2: i_q ripple of the FMPC with/without L_f.

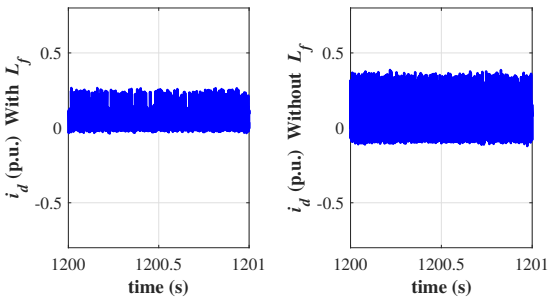

Fig. 18. Case 2: i_d ripple of the FMPC with/without L_f.

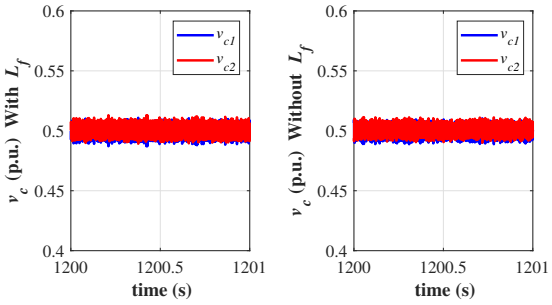

Fig. 19. Case 2: DC-link capacitor ripple of the FMPC with/without L_f.

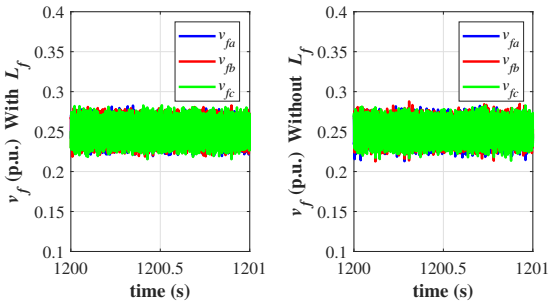

Fig. 20. Case 2: Flying capacitor ripple of the FMPC with/without L_f.

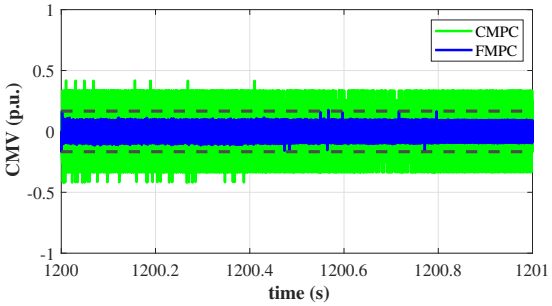

Fig. 21. CMV comparison between the proposed FMPC and CMPC.

VII. Conclusion

This paper proposes a fast MPC method with mitigated CMV and without weighting factors. The proposed method is implemented on a 5L-ANPC inverter-fed CAFPM motor drive in an electric aircraft propulsion system. The proposed FMPC method consists of three steps. The first step utilizes a deadbeat approach to calculate the reference dq voltage vector based on the discrete-time model of the CAFPM motor. In the second step, a set of voltage vectors with limited CMV values of $\pm\frac{V_{dc}}{6}$ is introduced. As a result, the CMV value is mitigated, and its adverse effects are relieved. The space vector diagram of the 5L-ANPC inverter is systematically sectioned, and according to the angle and magnitude of the calculated reference voltage vector, a set of candidate voltage vectors is selected for the iterative search. Therefore, the computational burden of the proposed method is reduced. In the third step, hierarchical cost functions are adopted to eliminate the weighting factors, where the first layer selects the optimum voltage vector, and the second one finds the optimum switching state. Meanwhile, the voltage across the DC-link and flying capacitors is balanced. Due to its reduced computational burden, the proposed method can use a higher sampling frequency, leading to its desirable performance in motor-drive systems with low inductance. The performance of the proposed method is studied in the aircraft takeoff and cruise modes in terms of speed, torque, current, and DC-link and flying capacitor voltage ripples.

References

[1] V. Madonna, P. Giangrande, and M. Galea, "Electrical power generation in aircraft: Review, challenges, and opportunities," *IEEE Transactions on Transportation Electrification*, vol. 4, no. 3, pp. 646–659, 2018.

[2] T. C. Cano, I. Castro, A. Rodríguez, D. G. Lamar, Y. F. Khalil, L. Albiol-Tendillo, and P. Kshirsagar, "Future of electrical aircraft energy power systems: An architecture review," *IEEE Transactions on Transportation Electrification*, vol. 7, no. 3, pp. 1915–1929, 2021.

[3] C. E. Jones, P. J. Norman, S. J. Galloway, M. J. Armstrong, and A. M. Bollman, "Comparison of candidate architectures for future distributed propulsion aircraft," *IEEE Transactions on Applied Superconductivity*, vol. 26, no. 6, pp. 1–9, 2016.

[4] J. F. Gieras, R.-J. Wang, and M. J. Kamper, *Axial flux permanent magnet brushless machines*. Springer Science & Business Media, 2008.

[5] F. Nishanth, J. Van Verdeghem, and E. L. Severson, "A review of axial flux permanent magnet machine technology," *IEEE Transactions on Industry Applications*, vol. 59, no. 4, pp. 3920–3933, 2023.

[6] T. Bingham, M. Moore, T. De Caux, and M. Pacino, "Design, build, test and flight of the world's fastest electric aircraft," *IET Electrical Systems in Transportation*, vol. 12, no. 4, pp. 380–402, 2022.

[7] F. Marcolini, G. De Donato, F. G. Capponi, M. Incurvati, and F. Caricchi, "Novel multiphysics design methodology for coreless axial flux permanent magnet machines," *IEEE Transactions on Industry Applications*, 2023.

[8] K. Wang, Z. Zheng, L. Xu, and Y. Li, "An optimized carrier-based pwm method and voltage balancing control for five-level anpc converters," *IEEE Transactions on Industrial Electronics*, vol. 67, no. 11, pp. 9120–9132, 2019.

[9] C. Li, S. Wang, Q. Guan, and D. Xu, "Hybrid modulation concept for five-level active-neutral-point-clamped converter," *IEEE Transactions on Power Electronics*, vol. 32, no. 12, pp. 8958–8962, 2017.

[10] Y. Yang, H. Wen, M. Fan, M. Xie, S. Peng, M. Norambuena, and J. Rodriguez, "Computation-efficient model predictive control with common-mode voltage elimination for five-level anpc converters," *IEEE Transactions on Transportation Electrification*, vol. 6, no. 3, pp. 970–984, 2020.

[11] F. Y. Notash, J. Rodriguez, and S. Tohidi, "One beat delay predictive current control of a reduced-switch 3-level vsi-fed ipmsm with minimized torque ripple," in *2021 IEEE International Conference on Predictive Control of Electrical Drives and Power Electronics (PRECEDE)*. IEEE, 2021, pp. 519–523.

[12] F. Y. Notash and J. He, "Simplified model predictive control of 5l-anpc inverter-fed afpm motor drives in electric aircraft propulsion systems," in *2024 IEEE Transportation Electrification Conference and Expo (ITEC)*. IEEE, 2024, pp. 1–7.

[13] M. Vatani, Y. Chulaee, A. Mohammadi, D. R. Stewart, J. F. Eastham, and D. M. Ionel, "On the optimal design of coreless afpm machines with halbach array rotors for electric aircraft propulsion," in *2024 IEEE Transportation Electrification Conference and Expo (ITEC)*. IEEE, 2024, pp. 1–6.

[14] F. Y. Notash, B. Luckett, and J. He, "A simplified fixed switching frequency model predictive control for an afpm motor drive in a distributed electric aircraft propulsion system," in *2023 IEEE Energy Conversion Congress and Exposition (ECCE)*. IEEE, 2023, pp. 4690–4697.

[15] P. Cortes, J. Rodriguez, C. Silva, and A. Flores, "Delay compensation in model predictive current control of a three-phase inverter," *IEEE Transactions on Industrial Electronics*, vol. 59, no. 2, pp. 1323–1325, 2011.

[16] Y. Yang, J. Pan, H. Wen, X. Zhang, M. Norambuena, L. Xu, and J. Rodriguez, "Computationally efficient model predictive control with fixed switching frequency of five-level anpc converters," *IEEE Transactions on Industrial Electronics*, vol. 69, no. 12, pp. 11 903–11 914, 2021.